AD A111306

DTIC FILE COPY

(2)

A

Technology Service Corporation

82 01 11 079

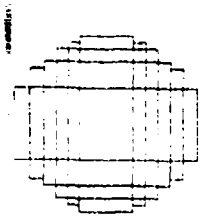

Technology Service Corporation

Washington Operations: 8555 Sixteenth Street, Silver Spring, Maryland 20910 Phone: (301) 565-2970

Ref: TSC-W25-227/mm
A2539211

DOPPLER SPECTRA OF RADAR CLUTTER

30 November 1981

Prepared by Wayne Rivers

Prepared under:

Contract N60921-80-D-A131
Delivery Order 0509
CDRL Item No. A002

Prepared for:

Naval Surface Weapon. Center
Weapon Control Division, Code N-53
Dahlgren, Virginia 22448

TABLE OF CONTENTS

ABSTRACT

Radar clutter spectra having sufficient dynamic range and resolution to permit shape estimation are reviewed. All are found to be distinctly non-Gaussina. A clutter scatterer motion model that includes correlation of velocities is defined and supported by empirical data for the case of wind fields. The Doppler spectra of scatterers with correlated motions are computed. Improvement factors for binominal-weighted moving-target indicators (MTI) are computed for several analytic spectrum functions that bound various observed features of empirical spectra.

1.0 INTRODUCTION AND SUMMARY

1.1 INTRODUCTION

In Barlow's 1949 tutorial paper on Doppler radar [1] he introduced the notion of clutter spectrum. He stated that the power spectra of land, sea, rain, and chaff were all approximately Gaussian,

$$S(f) = \exp \{- a f^2/f_o \} , \qquad (1)$$

and he gave typical values of the constant a for each. Since that time, almost all analysis of radars and most interpretation of experimental observations of clutter proceed under the assumption of a Gaussian shaped spectrum. The fluctuation spectra produced in radar signals by antenna scanning or by linear shear are reasonably expected to be approximately Gaussian. But we are talking here about the intrinsic motion of the scatterers which is the limiting spectral spreading mechanism for noiseless non-scanning radar.

Since 1950 almost all papers that have 'Doppler Spectrum' in their titles report only the standard deviation of the spectrum width, and occasionally a few curves spanning 10 dB or so of dynamic range. With so shallow a range, no shape determination can be made. But whenever spectra were analyzed to reveal spectral fall off to 20 dB or more, the spectral shapes have been distinctly non-Gaussian. Rather, a shape more simply exponential is suggested:

$$(f) = \exp \{-b|f|\} \qquad (2)$$

This shape cannot be explained by physical models of scatterer motion involving either linear shear or uniform and independent Gaussian random motion of scatterers. Some other mechanism of correlated motion must dominate. Note that we expect that motion must dominate in some cases, rather than amplitude modulation of the scatterers' cross sections, so a motion based model is first most attractive for attention.

It is the purpose here to explore a scatterer motion model that predicts a spectrum more like observed clutter spectra than the traditional Gaussian assumption.

The motion model chosen for entry is a Wiener process, with the radial velocity as the process variable and the transverse position in the radar beams as the parameter.

1.2 Summary

Reported empirical radar clutter spectra having dynamic range of 20 dB or greater are reviewed. It is found that none of these spectra have shapes that are reasonably interpreted as Gaussian. Rather, they all have two features not characteristic of the classical Gaussian shape. Their shape near zero modulation frequency shows a peak, rather than a rounded nose, and the falloff of spectral density at higher modulation frequencies is much slower than Gaussian. For the first 20 dB or so of density, the shapes are approximately exponential in modulation frequency.

A motion model is postulated to account for the observed spectra, Clutter scatterers are assumed moving such that their radial velocities are correlated. The correlation is introduced by assuming that the differences in radial velocities of scatterers separated by a given distance is a Weiner process in the separation variable. Spectra of this model are computed and compared with the data base for both coherent and noncoherent cases. The spectra computed from the model have the same sharp peak as the data, but the match to the shape in the high-frequency region is indeterminate.

Several analytic functions having features bounding those of the empirical spectra are used to compute binomial-weight MTI improvement factors, under the assumption of equal -3 dB widths for all spectra. It is shown that great differences in improvement factor can be expected under the various shape assumptions. The physical reasonableness of the illustrative spectral functions is assessed.

A major conclusion is that because of the historical bias toward a Gaussian clutter spectrum shape, the interpretation of clutter spectral width constants may have been in error by as much as a factor of 2.5.

1.3 Discussion

The existence of clutter spectra having peaked shapes near zero modulation frequency, rather than rounded, brings into question the accuracy of all previous estimates of clutter spectrum widths which were made under the Gaussian assumption for shape. Direct measurement of clutter spectrum bandwidth with filters must be corrected differently for filter bandwidth under Gaussian and non-Gaussian assumptions. Indirect measurement of bandwidth, via a decorrelation time, not only requires appropriate account of shape effects but also of the effect of noise near zero lag. It seems probable that some pervious measurements reported for spectral widths may be in error by as much as a factor of 2.5, depending on how the estimate of width was made. This error is somewhat larger than one would expect spectra to vary under the same nominal observing conditions. Without a thorough review of the procedures used in previously reported clutter bandwidth surveys to transform primary measured data to the standardized width constants, much more about the bias of error cannot be said at this time.

In the theoretical modeling of clutter spectra presented herein, some variation of wind shear correlation was investigated to see what its effect was on the tails of modulation spectra. Over the range of correlation parameter values allowed by observed wind field data, the predicted spectrum tails still fall off faster than observed clutter. It is interpreted that a scatterer lifetime model is needed in addition to the motion model to add power at the frequencies to the theoretical total spectrum, along the lines suggested by the signal analyses in Reference 2.

The existence of high-frequency tails in the spectra, compared to the Gaussian prototype, has implications for radar MTI design and performance prediction. In Appendix B are shown results of calculations of improvement factor for 3-pulse and 4-pulse binomial weighted MTI processors under the assumptions of clutter spectral shape from Gaussian to the extreme f** (-2) and the same -3 dB bandwidth for each analytic function. There it can be seen that the effect of the tails is to limit the performance achievable

with 4 pulses to about that with 3 pulses, and to temper expectations about the improvement achievable to lower levels than the ideal Gaussian would allow. Given such hypothetical non-Gaussian spectra, increased improvement can only come using a bank of bandpass filters appropriately weighted to the spectrum or a non-binomial weighted MTI.

Appendix C examines the hypothetical spectra, each of which, except the Gaussian, has some feature relatable to the empirical data, for reasonableness in regard to physical considerations. Finiteness of power in the process, causality, and existence of derivatives are considered. It is concluded that, of the set examined, only a spectrum of the form exp(-f**α), where $\alpha<1$, passes the tests. For values of α in the neighborhood of 0.85 that function also approximately represents the empirical data.

2.0 EMPIRICAL CLUTTER SPECTRA

Wide dymanic-range spectra have been published for back-scattering from foliage and from sea waves. None has been found published for precipitation. All of the coherent spectra found so far for precipitation have usable dynamic range of the order of 10 dB and uncertain frequency resolution. Here are presented three foliage clutter examples and one sea backscatter and one sea forward-scatter example. All of the spectrum plots are of power per unit handwidth in dB against modulation frequency on a linear scale.

2.1 Land Clutter Spectra

Figure 1 shows two coherent spectra of foliage return at X band [2]. The curves were normalized in frequency to cross at their -15 dB points. The publishing authors had plotted the spectra against the logarithim of frequency, thus observing the simple shape and especially the slope near zero frequency. Wind speeds were light, 5 kt or less in all three cases. The cospectra and cross-spectra were computed separately and showed that Doppler modulation dominated at levels above the -15 dB point but amplitude modulation contributed below that level. Amplitude modulation is presumed to be caused by rotation of the scatterers in the wind.

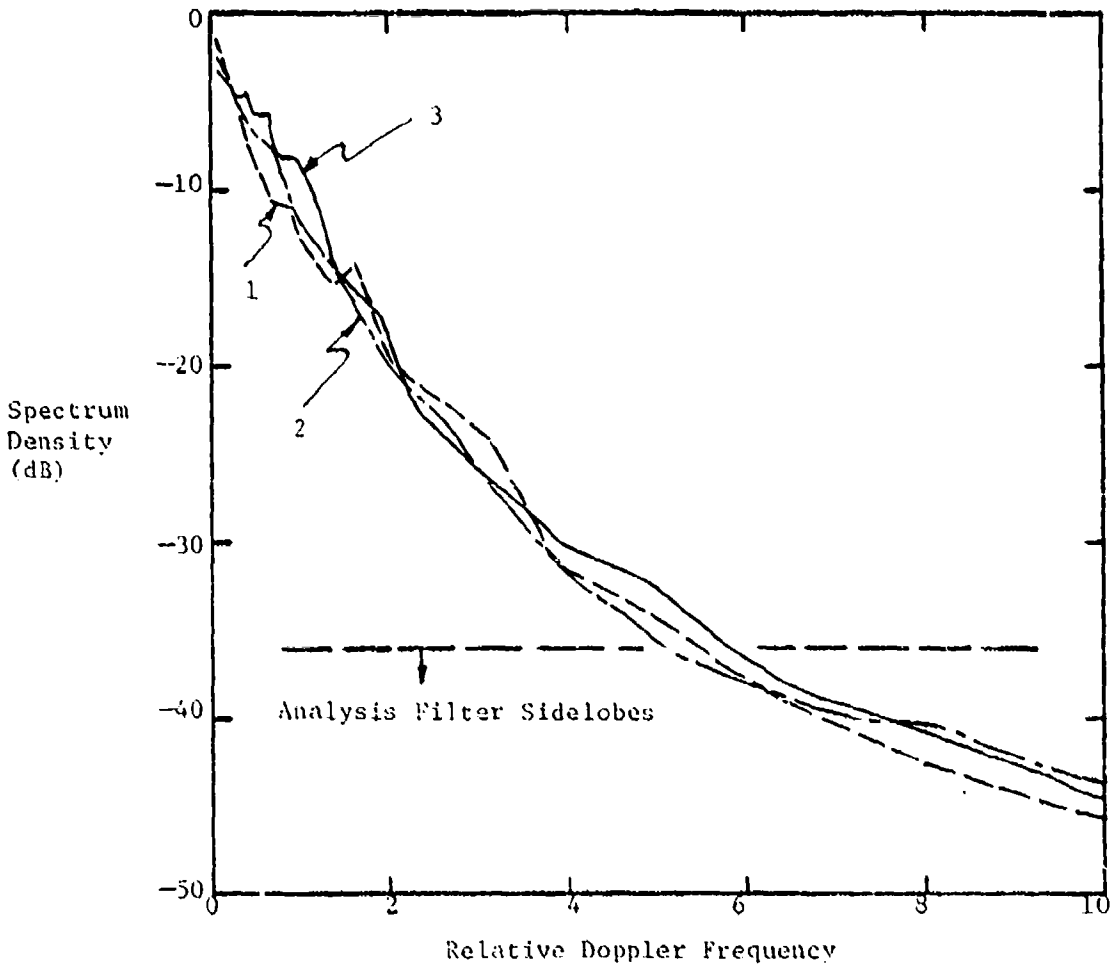

Figure 1. Kapitanov's coherent spectra of forest at x-band. [2]
Spectrum widths are

1 - 0.8 Hz

2 - 1.8 Hz

3 - 8.5 Hz

Another example of radar backscatter from foliage is shown in Figure 2 in the form originally published [3]. In this case, the frequency analysis of non-coherent video was done with a rectangular time window, which produces sidelobes in frequency down only 13 dB peak near the mainlobe and of the order of -42 dB at f=40 Hz and -48 dB at 80 Hz. The spectrum from Figure 2, which is plotted against frequency on a logarithmic scale, is replotted on a linear frequency scale, in Figure 3.

A second example of noncoherent spectrum of land return is shown in Figure 4 and 5, the first against log frequency and the second against linear frequency [4]. Again there is a tailing departure from simple exponential but at a much lower level than predicted in Appendix A, and the slope near zero frequency does not level in an obvious manner.

2.2 Sea Clutter Spectra

Figures 6 and 7 show two examples of non-coherent spectra of radar sea return [5]. Here, over the somewhat limited dynamic range of 15 to 18 dB, the data can be viewed as definitely non-Gaussian. But whether the tail of the spectrum at high frequencies falls off slower as suggested by the other empirical cases cannot be known.

The remaining empirical spectrum example is shown in Figures 8 and 9. There, the coherent spectrum of L-band waves forward-scattered from a rough water surface is shown, along with the shape of the analysis filter [6]. Figure 8 details the spectrum over the upper 30 dB, and Figure 9 shows it for a wider dynamic range. The broadening of the spectrum below -90 dB is believed caused by a combination of interference and intermodulation in the input of the spectrum analyzer. The suggestion is strong here of an exponential shape down 50 dB or so, followed by a departure from the constant slope toward higher power.

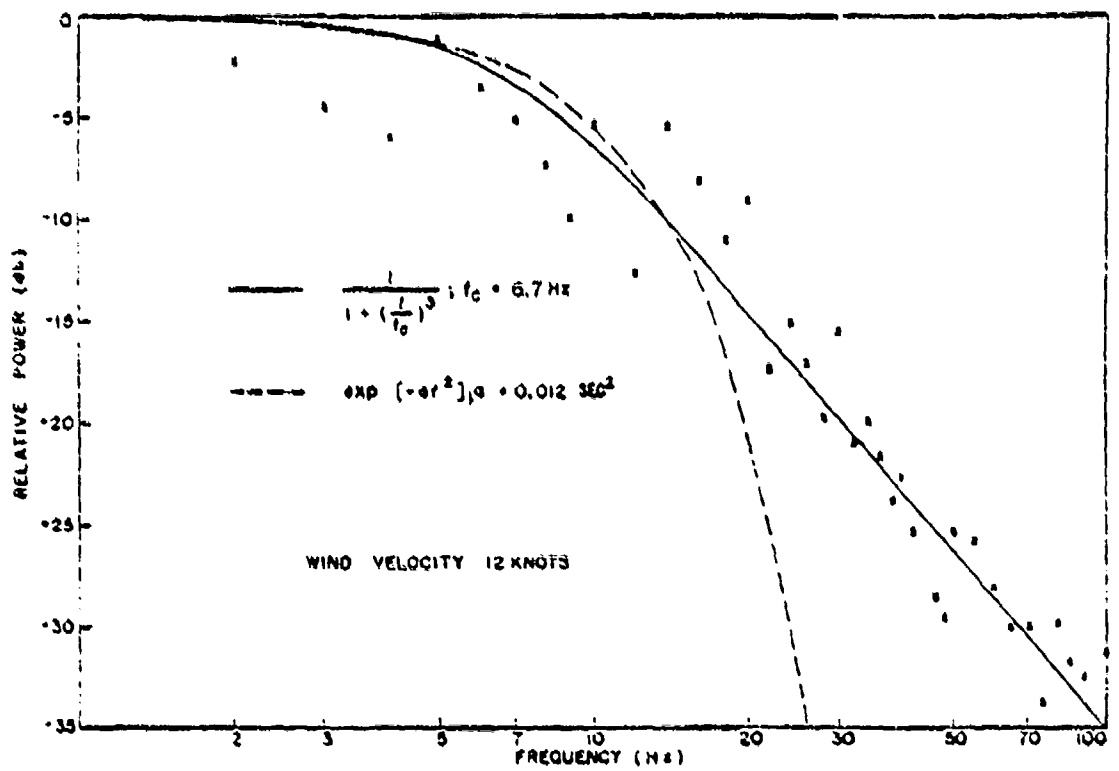

Figure 2. Noncoherent spectrum of foliage return at X-band. [3]

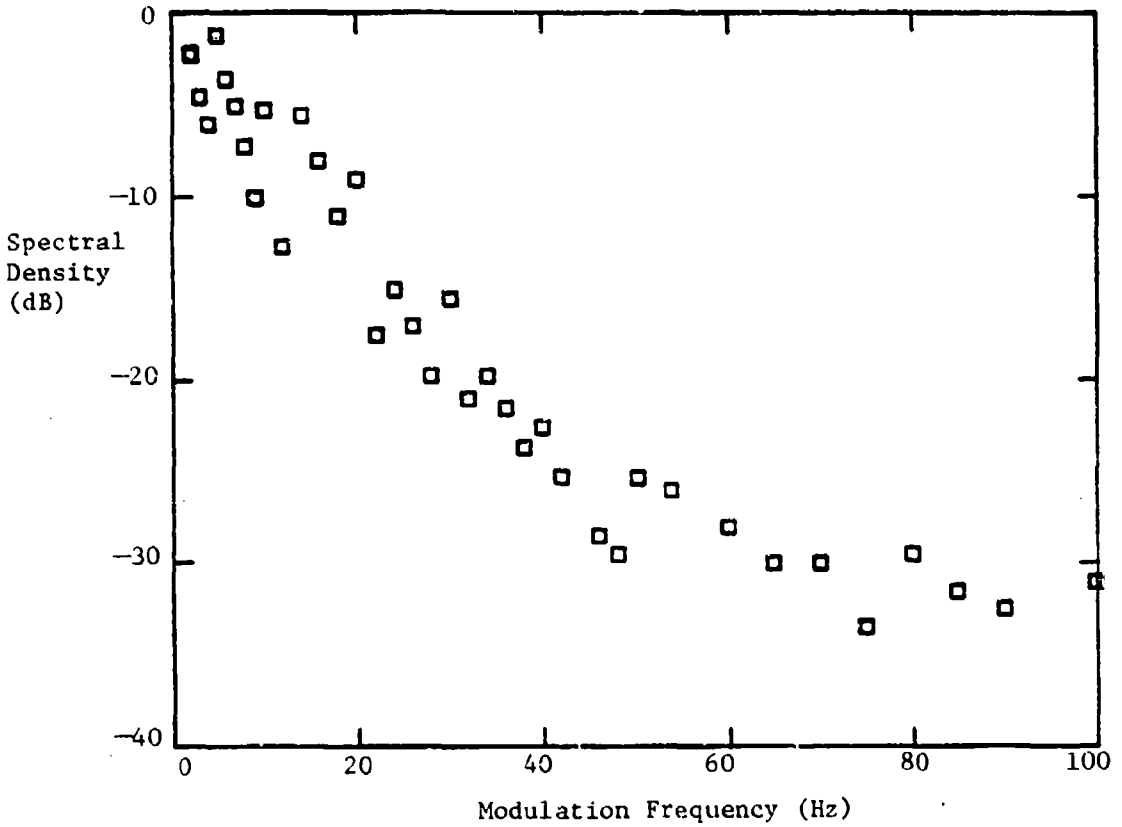

Figure 3 Non-Coherent Spectrum of Foliage at X Band [3]

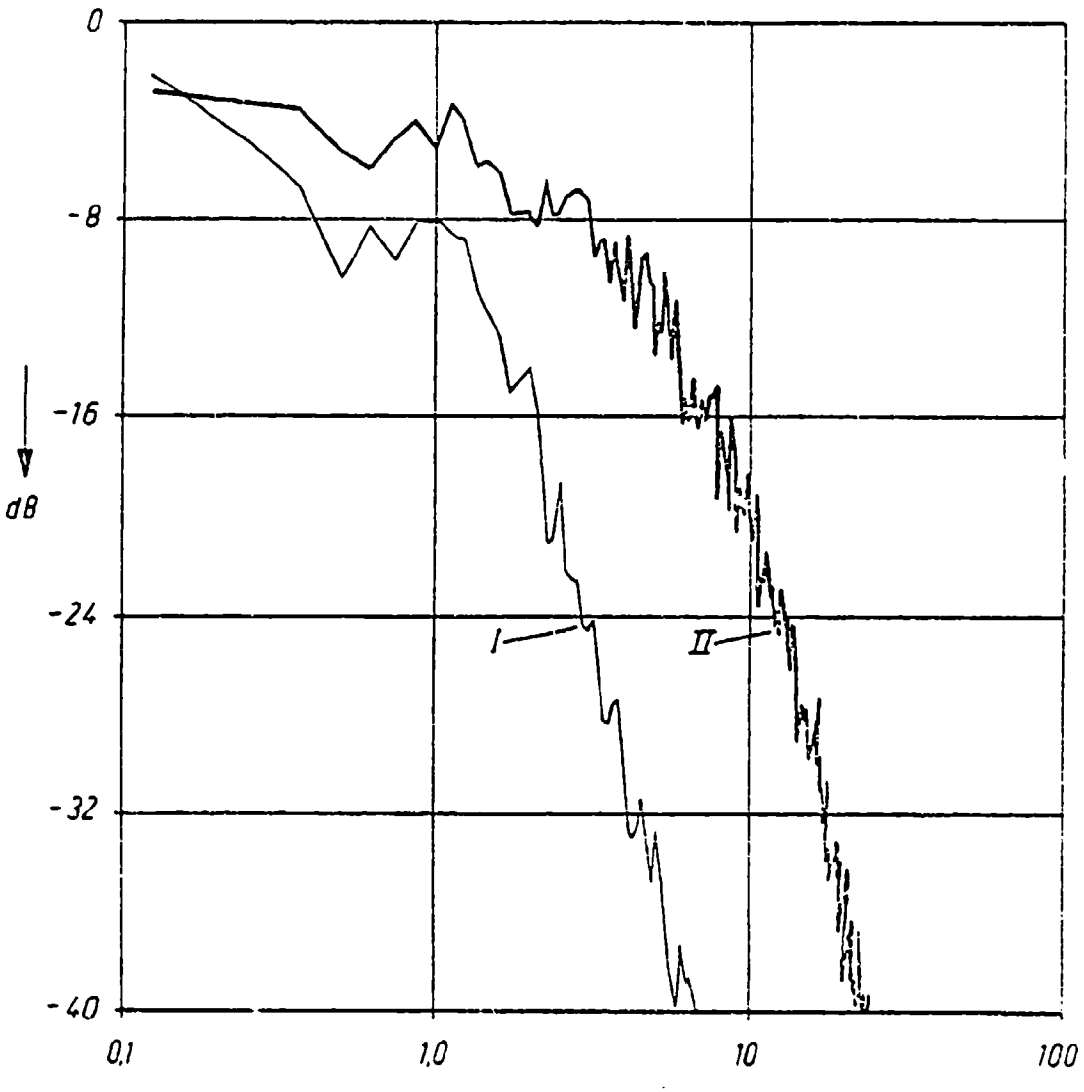

Frequency spectrum of the fluctuating component in a measurement of 100 secs. Wheat field, 23 July 1970

I. No wind,

II. Wind speed between 2.4 and 3 m/sec.

Figure 4. Facsimile of data from de Loor and Jurriens [4] Radar at x-band, HH polarization

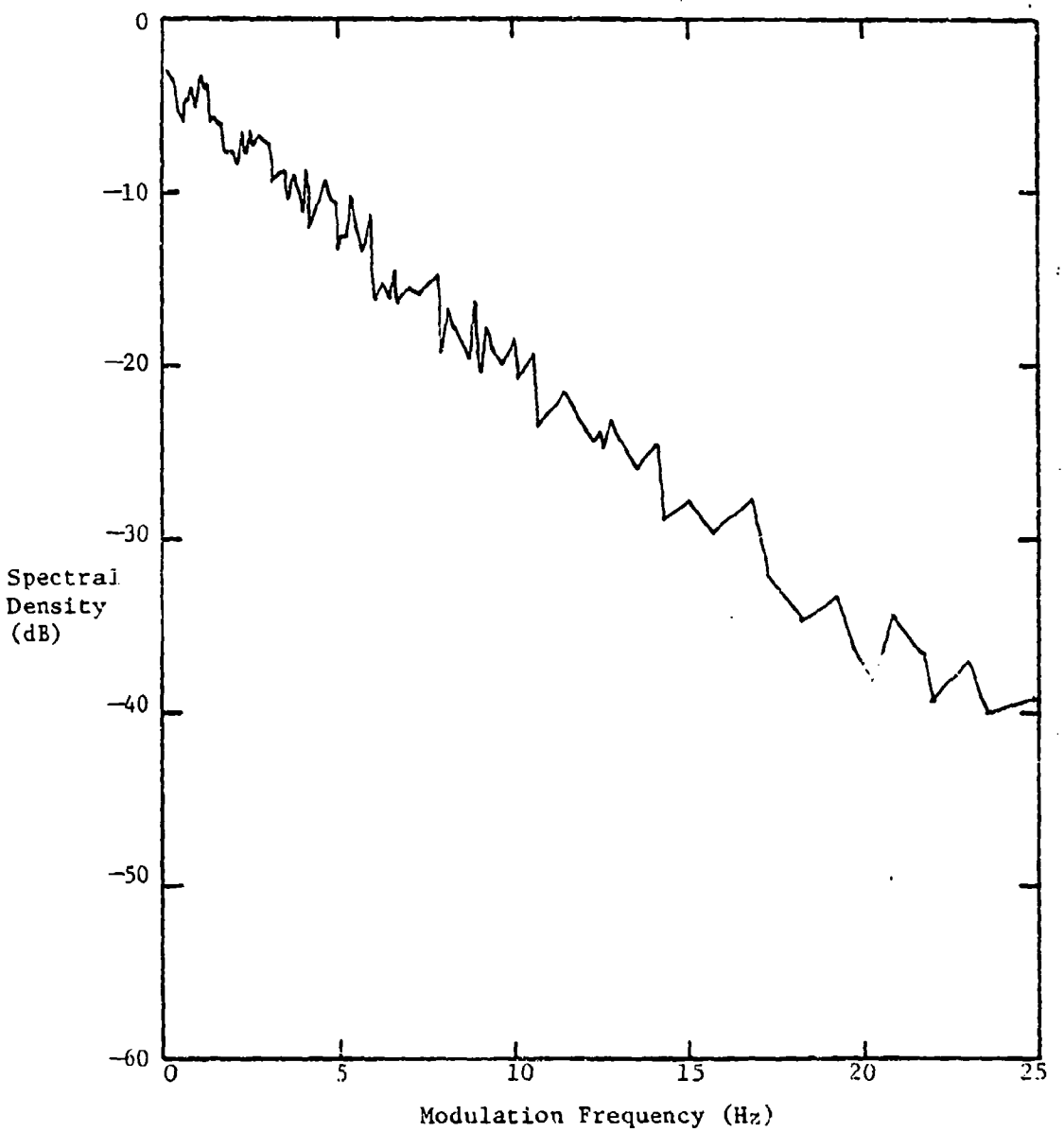

Figure 5. Noncoherent spect of wheat field at x-band, wind speed 2.4-3 m/s ata from Figure 4-II transformed here to linear frequency scale. [4]

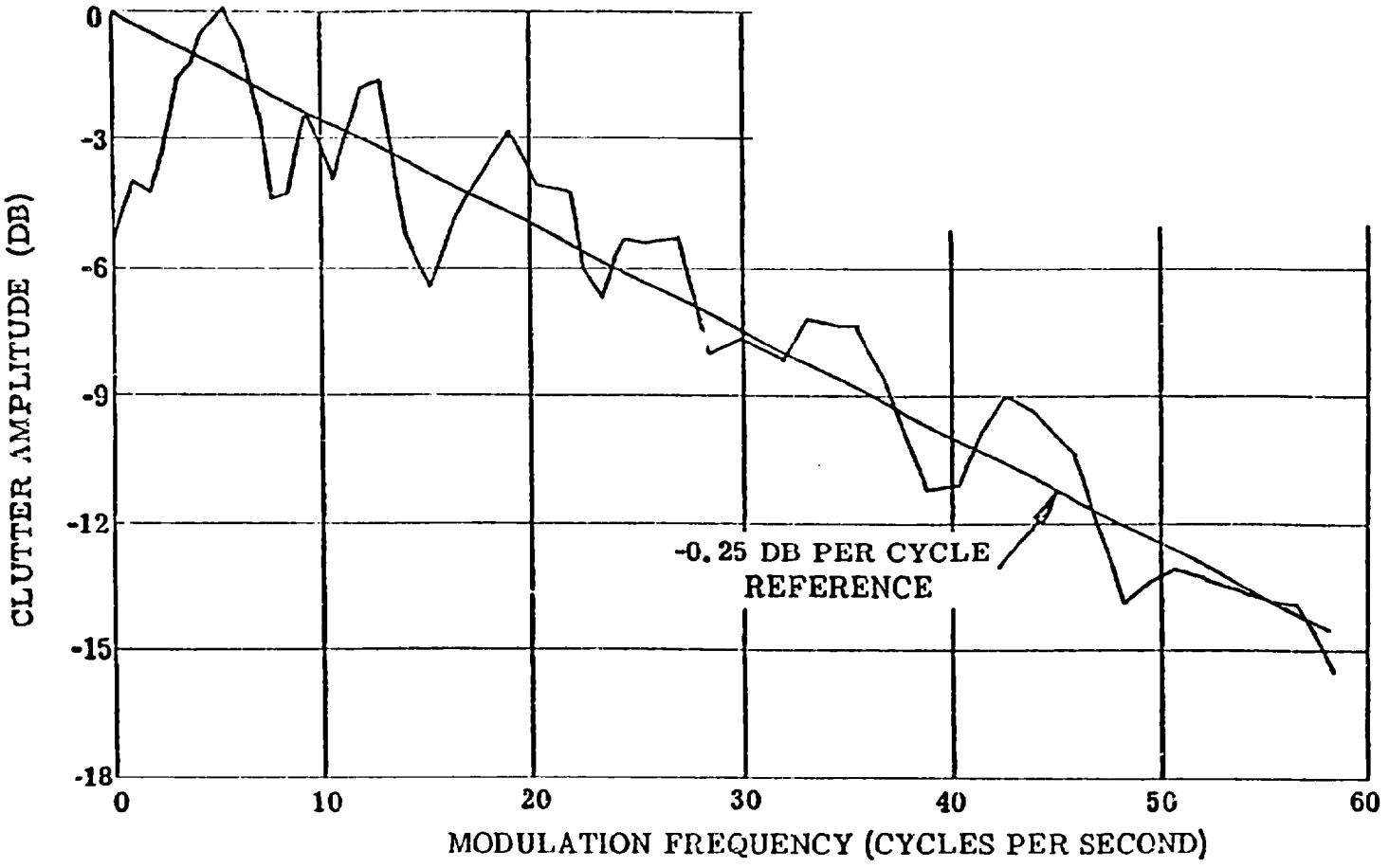

Figure 6. Noncoherent spectrum of radar sea backscatter [5].

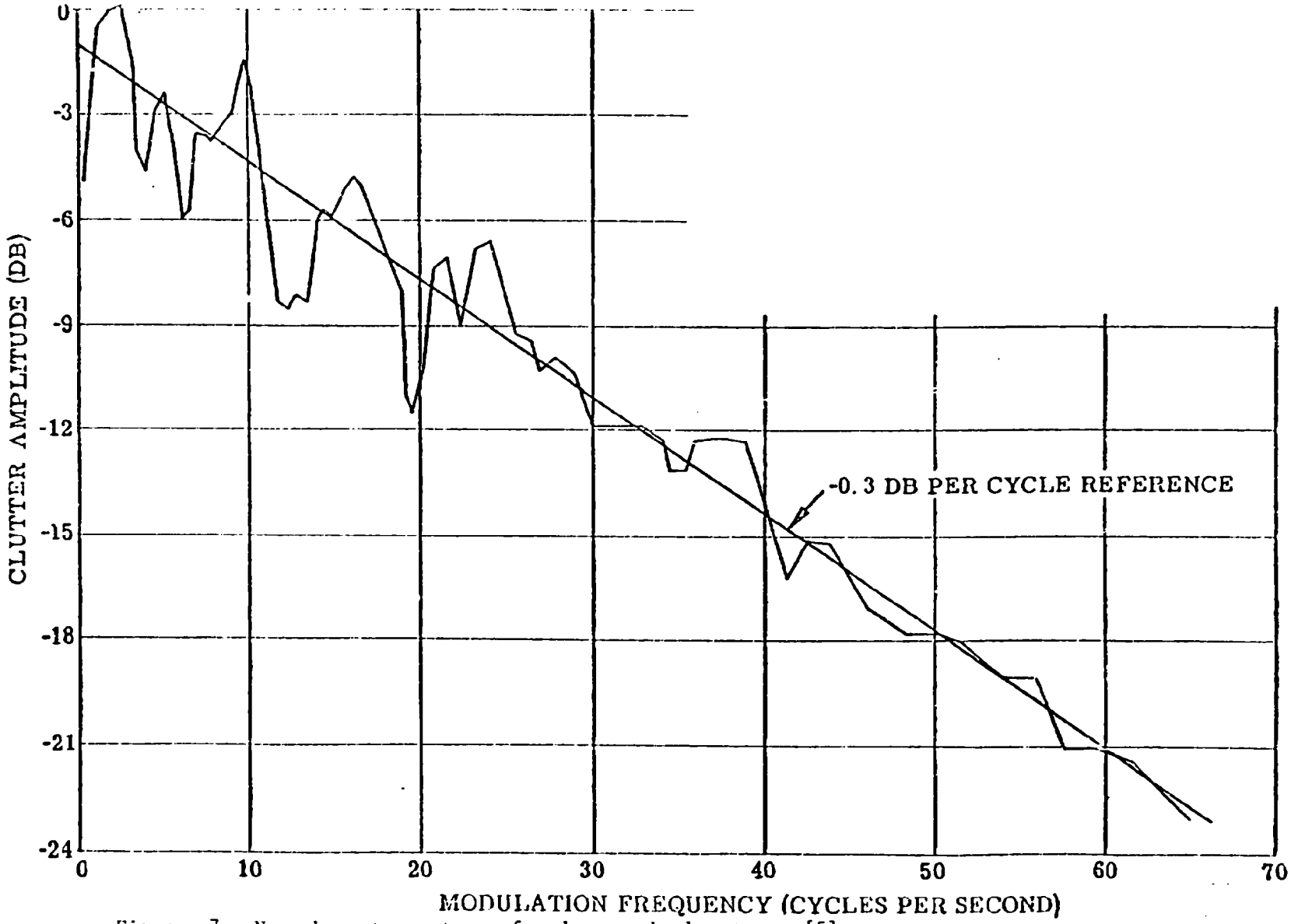

Figure 7. Noncoherent spectrum of radar sea backscatter [5].

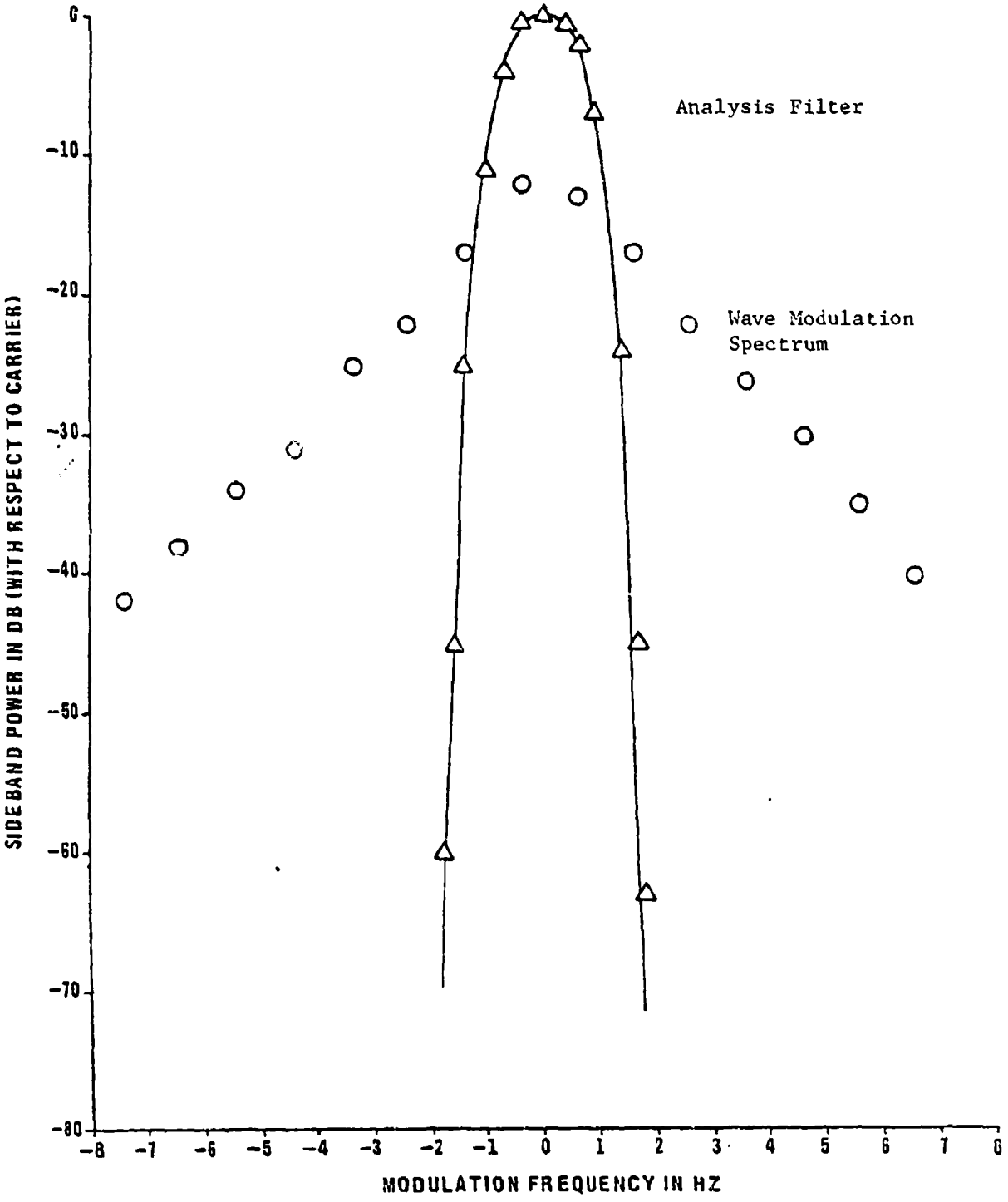

Figure 8. Coherent spectrum of L-band wave reflected from rough water surface at vertical incidence [6] .

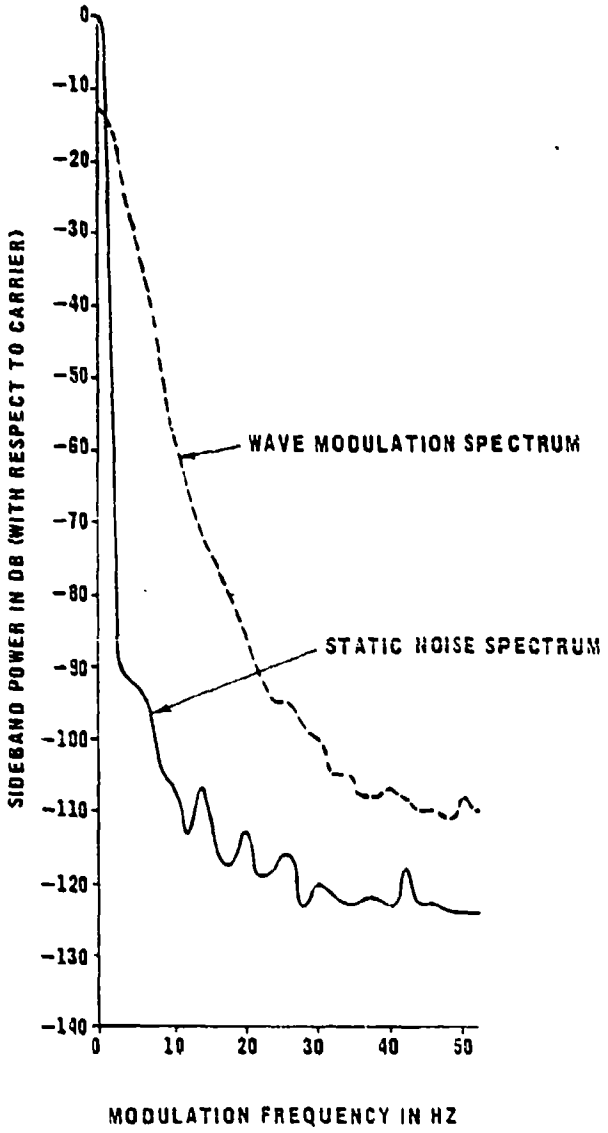

Figure 9. Coherent spectrum of L-band wave reflected from rough water surface at vertical incidence [6]

3.0 A MOTION MODEL FOR CLUTTER SPECTRA

Clutter scatterer velocities seem to be Gaussian distributed. If their motion were independent, one would expect that the spectrum of backscatter signals would also be Gaussian. This logic may underlie the historic interpretation of observed spectra as being Gaussian shaped. But, there is strong evidence that motion independence does not exist. Where the correlation of scatterer motions has been measured, it has been found that the scatterer velocities are approximately Wiener distributed.

Here we define a Wiener-distributed velocity process, establish an empirical basis for its reasonableness in one case (a wind field), and compute coherent Doppler specta.

3.1 The Wiener Process

A random process $x(t)$ is said to be a Wiener process if it satisfies these conditions [7]:

(a) $x(t)$, $t>0$, has stationary independent increments for incremental t;

(b) For every $t>0$, $x(t)$ is normally distributed;

(c) For all $t>0$, $E(x(t)) = 0$;

(d) $x(0) = 0$.

$$\text{Var}\,[x(t) - x(s)] = \sigma^2\,|t-s|, \tag{3}$$

in which the simple parameter σ^2, plus the four properties above, completely describe the process.

3.2 An Example of Scatterer Motion

Atmospheric winds containing precipitation seem to have properties close to the Wiener process. Consider these definitions.

- Air moves horizontally with an average vector u oriented along the x axis. Thus, $\vec{\bar{u}} = \bar{u}_x \vec{x}$

- Turbulence causes the local wind components to vary, in particular with displacement of observing position along the z(vertical) axis. Thus, $\vec{u} = u_x(z)\vec{x} + u_y(z)\vec{y}$

- The longitudinal wind speed, $u_x(z)$, has both constant and fluctuation components. Thus, $u_x(z) = \bar{u}_x(z) + v_x(z)$. In the transverse direction, $u_y(z) = v_y(z)$

- A Structure Function is the mean of the product of spatial difference of two wind components. Thus, for the longitudinal co-structure function for lag is the vertical direction,

$$D_{xx}(\delta z) = \overline{\left[u_x(z+\delta z) - u_x(z)\right]^2} \tag{4}$$

Also, $$D_{yy}(\delta z) = \overline{\left[u_z(z+\delta z) - u_y(z)\right]^2} \tag{5}$$

and the general case is

$$D_{ij}(\ ) = \overline{\left[u_i(\vec{r}+\vec{r}_1) - u_i(\vec{r}_1)\right]\left[u_j(\vec{r}+\vec{r}_1) - u_j(\vec{r}_1)\right]}$$

- Wind shear is the difference in a component of the wind caused by displacement normal to the component's direction. Thus, "vertical wind shear" is the term denoting the vector change in horizontal wind for displacement along the horizontal axis: $\vec{\Delta u}(z) = \Delta u_x(z)\vec{x} + \Delta u_y(z)\vec{y}$.
  Also $\Delta u_x(z) = \overline{\Delta u}_x(z) + \Delta v_x(z)$ and $\Delta u_y(z) = \Delta v_y(z)$.

Observers of the atmosphere have established these properties of wind shear. Essenwanger [8] has established that

(a) the fluctuation components of the wind (turbulence) are Gaussian, with the standard deviation of the longitudinal component about 2.5 times that of the transverse component.

(b) The fluctuation components of the vertical shear are Gaussian, with equal standard deviations.

(c) The average vertical shear is about one third the standard deviation of the longitudinal component.

(d) The standard deviation of vertical shear increases proportional to the square root of vertical separation.

One of Essenwanger's data sets is plotted in Figure 10. There the logarithm of shear variance is plotted against the logarithm of vertical separation. The slope is seen to be about 1.1 for separations less than 400m, about 0.7 above 400m, with an average of 1.0 over the maximum 1000m span plotted.

Melnichuk [9] analyzes shear in terms of the longitudinal and transverse structure functions. He finds for the longitudinal component near the ground a slope of 1.2 below a break at 400m vertical separation and about 0.5 above, up to his maximum analyzed value of 760m. But at that low altitude (base of observations was 130m altitude), the transverse component's slope broke at 150m separation, decreasing from 1.0 below to nearly 0 above.

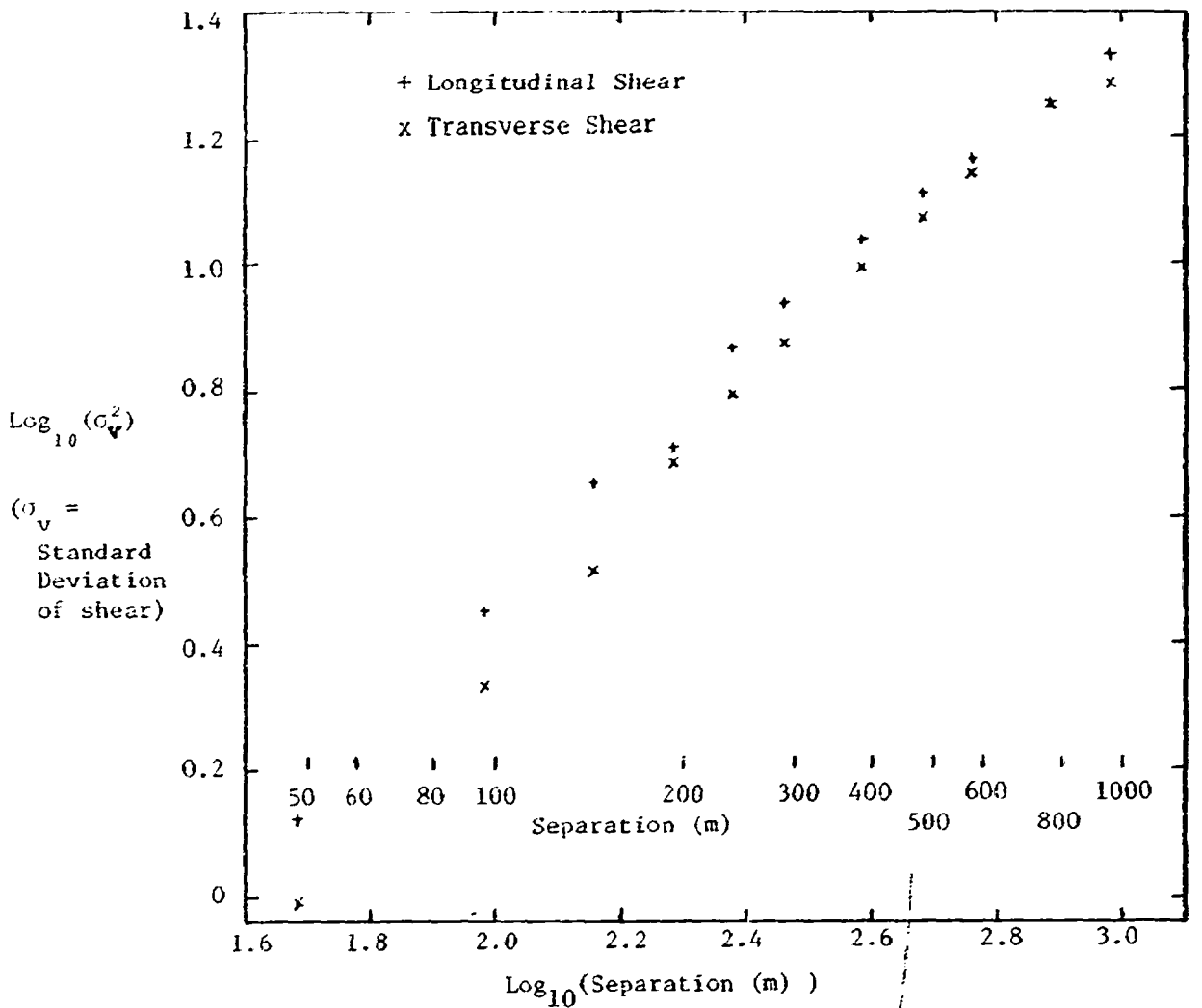

Figure 10. Variation of Vertical Shear Variance with Separation [8]

The slope referred to above is the parameter q in the following empirical laws:

$$\sigma_v^2(z) = A\, z^q$$
$$D(z) = B\, z^q \tag{6}$$

Both authors referred to above heartily subscribe to such laws.

3.3 Doppler Spectrum of a Wiener Velocity Process

Let a radar beam illuminate wind-driven scatterers. Choose the center of the beam as a reference point, at position $z=z_o$. Assume that the wind velocity relative to the average wind in the radial direction is representable by a Wiener process in the variable z. Then $v(z) - v(z_o)$ is normal with a zero mean and a variance

$$\mathrm{Var}[v(z) - v(z_o)] = \sigma^2 \, |z-z_o| . \tag{7}$$

The parameter σ^2 is the single one necessary to define the distribution of this shear process.

Assume further that the average reflectivity of scatterers in a layer (z, z+dz) is constant with z. Then, the clutter power moving with doppler velocity (v, v + dv) is

$$S(v)\, dv = dv \int f(v, z)\gamma\, G(z)\, dz, \tag{8}$$

in which γ is the reflectivity in height interval dz and f(v,z) is the probability density function of v, given z. G(z) is the radar beam shape function.

The pdf of v is

$$f_v(v) = \frac{1}{\sqrt{2\pi}\,\sigma_v} \exp\left\{ - \frac{v^2}{2\,\sigma_v^{\,2}} \right\}, \tag{9}$$

in which $\sigma_v^{\,2}$ is the variance of v, here simplified to denote the difference in speeds, $v = v(z) - v(z_o)$. the variance $\sigma_v^{\,2} = \sigma^2 |z - z_o|$ is as in Formula 7.

Let the beam shape be Gaussian,

$$G(z) = \exp\left\{ - \frac{z^2}{2\sigma_B^{\,2}} \right\} \tag{10}$$

so that its 3 dB point occurs at

$$z_{0.5} = \sqrt{2 \ln 2}\,\sigma_B = 1.1774\,\sigma_B, \tag{11}$$

and its full width at half power is $2\sqrt{\ln 2}\,\sigma_B = 2.355\sigma_B$. The beam's one-dimensional area, or effective full width, is

$$W_z = \sqrt{2\pi}\,\sigma_B \tag{12}$$

and the total scattered power is

$$RCS = W_z\,\gamma = \sqrt{2\pi}\,\gamma\sigma_B. \tag{13}$$

Then, $S(v)\,dv = \int_{z=-\infty}^{\infty} \frac{1}{\sqrt{2\pi}\,\sigma_v} \exp\left\{-\frac{v^2}{2\sigma_v^2}\right\} dv\ \gamma \exp\left\{-\frac{z^2}{2\sigma_B^2}\right\} dz$

$$= \int_{-\infty}^{\infty} \frac{\gamma dv}{\sqrt{2\pi}\sigma} \frac{1}{\sqrt{|z|}} \exp\left\{-\frac{v^2}{2\sigma^2|z|} - \frac{z^2}{2\sigma_B^2}\right\} dz \qquad (14)$$

$$= \int_{0}^{\infty} \sqrt{\frac{2}{\pi}}\,\gamma \frac{dv}{\sigma} \frac{1}{z^{1/2}} \exp\left\{-\frac{v^2}{2\sigma^2 z} - \frac{z^2}{2\sigma_B^2}\right\} dz$$

The function $S^*(v) = 10 \log_{10}(S(v))$ is plotted in Figure 11 for three values of σ, $\sigma^2 = 0.25$, 1 and 4 $m^2/sec^2/m$. Also plotted there is a Gaussian function having small-lag decorrelation and total power equal to those values for the S(v) (solid) curve for which $\sigma=1$.

Two features of the function S(v) are noteworthy. First, the slope near v=0 is not zero, in marked contrast to the Gaussian function. Second, the slope is nearly constant, varying only 2:1 over 40 dB change in the spectral density.

An approximate expression for S*(v) is:

$$S^*(v) \approx -\frac{5}{\sigma\sqrt{\sigma_B}} \left[v - 0.3\ (2\sigma\sqrt{\sigma_B})^{-2/3}\ v^{5/3}\right]$$

$$+ 10 \log_{10}\left[\sqrt{\frac{2\sqrt{2}}{\pi}}\ \Gamma(1/4)\ \sqrt{\sigma_B}\ \frac{\gamma}{\sigma}\right] \qquad (15)$$

This expression matches Formula 14 numerically within 0.3 dB over the top 70 dB of the spectrum. Although not visible in Figure 2 the slope at v=0 is zero, and the radius of curvature is quite small. So by the time v reaches a few percent of the spectrum width at half peak power density the slope is significantly non-zero. However, except very near v=0, the slope of the spectrum is of the order of -5 dB per v unit for σ=1, (see Formula 15).

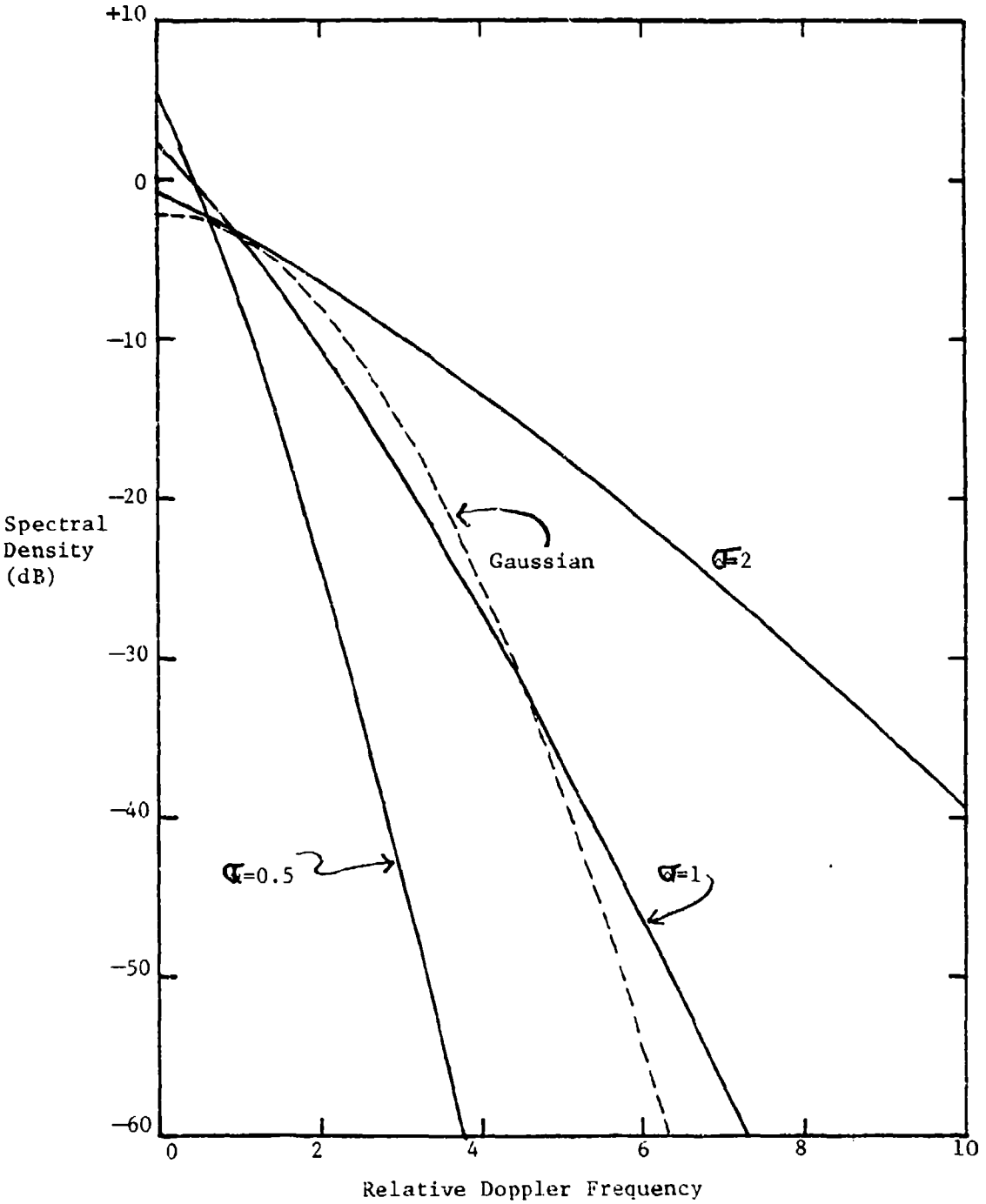

Figure 11. Spectrum of Doppler modulation by a Wiener-distributed velocity field.

3.4 Other Shear Variance Functions

Define the variance law for the wind shear to be

$$\mathrm{Var}[v(z) - v(z_o)] = \sigma^2 \, \delta z^q \qquad (16)$$

where the exponent q is now arbitrary but of the order of one, and $\delta z = |z - z_o|$. Using this law instead of Formula 7 and evaluating Formula 8 for the spectrum gives curves plotted in Figure 12. values of the exponent less than 1 are more curved, tending toward the Gaussian shape. Values greater than 1 tend toward exponential, and a value of 1.6 yields a nearly straight exponential spectrum.

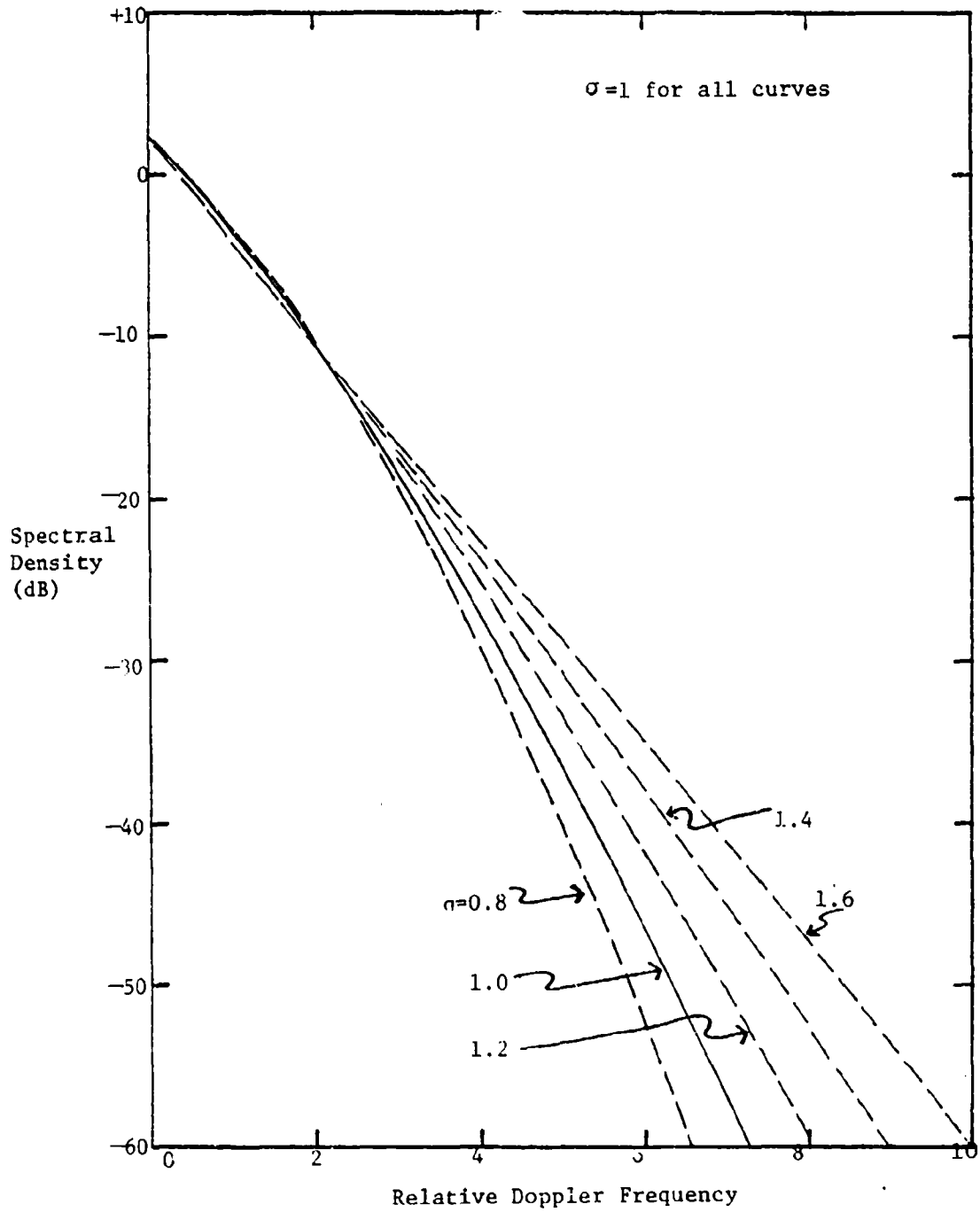

Figure 12. Spectrum of Doppler modulation by scatterers in a modified Wiener-like velocity field.

4.0 REFERENCES

1. "Doppler Radar," E. J. Barlow, Proceedings of the IRE, Vol. 37, No. 4, April 1949.

2. "Spectra of Radar Signals Reflected from Forests at Centimeter Waves," V. A. Kapitanov, Yu. V. Mel'nichuk, and A. A. Chernov, Radio Engineering and Electronic Physics Vol. 18, September 1973 pages 1330-1338.

3. "A Clutter Attenuation Analysis," W. Fishbein, S. W. Graveline, and O. E. Rittenbach, Technical Report ECOM - 2808, March 1967, AD 665352.

4. "Radar Ground Returns - Part I: The radar backscatter of vegetations," G. P. deLoor and A. A. Jurriens, National Defense Research Organizations - TNO, report Ph. L. 1972-3, January 1972.

5. "Engineering Lab Results - Bumble Bee Homing, Pulse Clutter Investigations," A. H. Horn and C. T. Sears, Convair, Report CF-2367, May 1955.

6. "Modulation by Water Waves of Radar Return at Vertical Incidence," A. B. Abeling, W. Rivers and R. G. Shackelford, Georgia Institute of Technology Report A-366-2, November 1966.

7. Stochastic Processes, E. Parzen, Holden Day, Inc., 1962

8. "Statistical Parameters and Percentile Values for Vector Wind Shear Distributions of Small Increments," O. Essenwanger, Anchiv fur Meterologie, Geophysik und Bioklimatologie, Series A, Vol. 15, No. 1 1965, pages 50-61.

9. "Doppler Radar Measurements of Turbulence in Precipitations," Zu. V. Mel'nichuk, Fizika atmosfery i okeana, Vol. II, No. 7, 1966, pages 695-704.

APPENDIX A

NON-COHERENT SPECTRA OF EXPONENTIAL-SPECTRUM CLUTTER

A.1 Square-Law Envelope Detector

Assume a clutter signal with a coherent spectrum of the form:

$$S(f) = A \exp\left\{ - |f|/f_1 \right\} . \tag{A1}$$

After the signal is square-law "envelope detected", the spectrum of the non-coherent video signal, neglecting the d.c. component, is [A-1]

$$Sn(f) = \frac{1}{\pi} \int_{-\infty}^{\infty} A^2 \exp\left\{ - \left| \frac{s}{f_1} \right| \right\} - A^2 \exp\left\{ - \left| \frac{f-s}{f_1} \right| \right\} ds \tag{A2}$$

Using Figure A-1 as a guide, this integral breaks into 3 parts.

$$\begin{aligned} Sn(f) = & \frac{1}{\pi} \int_{-\infty}^{0} A^2 \exp\left\{ + \frac{s}{f_1} \right\} \exp\left\{ - \frac{f-s}{f_1} \right\} ds \\ & + \frac{1}{\pi} \int_{0}^{f} A^2 \exp\left\{ - \frac{s}{f_1} \right\} \exp\left\{ - \frac{f-s}{f_1} \right\} ds \\ & + \frac{1}{\pi} \int_{f}^{\infty} A^2 \exp\left\{ - \frac{s}{f_1} \right\} \exp\left\{ - \frac{s-f}{f_1} \right\} ds \end{aligned} \tag{A3}$$

for the case f>0.

$$S_n(f) = \frac{1}{\pi} A^2 \exp(-f/f_1) \int_{-\infty}^{0} \exp\{+2s/f_1\}\, ds$$

$$+ \frac{1}{\pi} A^2 \exp(-f/f_1) \int_{0}^{f} ds$$

$$+ \frac{1}{\pi} A^2 \exp(f/f_1) \int_{f}^{\infty} \exp\{-2s/f_1\}\, ds$$

$$S_n(f) = \frac{1}{\pi} A^2 \exp(-f/f_1)\,(fi/2) \left[\exp\{2s/f_1\}\right]_{-\infty}^{0}$$

$$+ \frac{1}{\pi} A^2 \exp(-f/f_1) f$$

$$+ \frac{1}{\pi} A^2 \exp(f/f_1)(-f_1/2) \left[\exp\{-2s/f_1\}\right]_{f}^{\infty}$$

$$S_n(f) = f_1 A^2 \exp\{-f/f_1\}/2\pi$$

$$+ fA^2 \exp\{-f/f_1\}/\pi$$

$$+ f_1 A^2 \exp\{-f/f_1\} \exp\{-2f/f_1\}/2\pi$$

$$S_n(f) = \frac{1}{\pi} A^2 \exp\{-f/f_1\}\,(f+f_1)$$

$$S_n(f) = \frac{A^2}{\pi f_1}(1+f/f_1) \exp\{-f/f_1\} \qquad \text{(A4)}$$

Formula A4 is plotted in Figure A-2 along with the coherent spectrum (A-1) for the case $f_1 = 1$, but the densities have been normalized by displacing the non-coherent curve upward by $10\log_{10}(\pi)$.

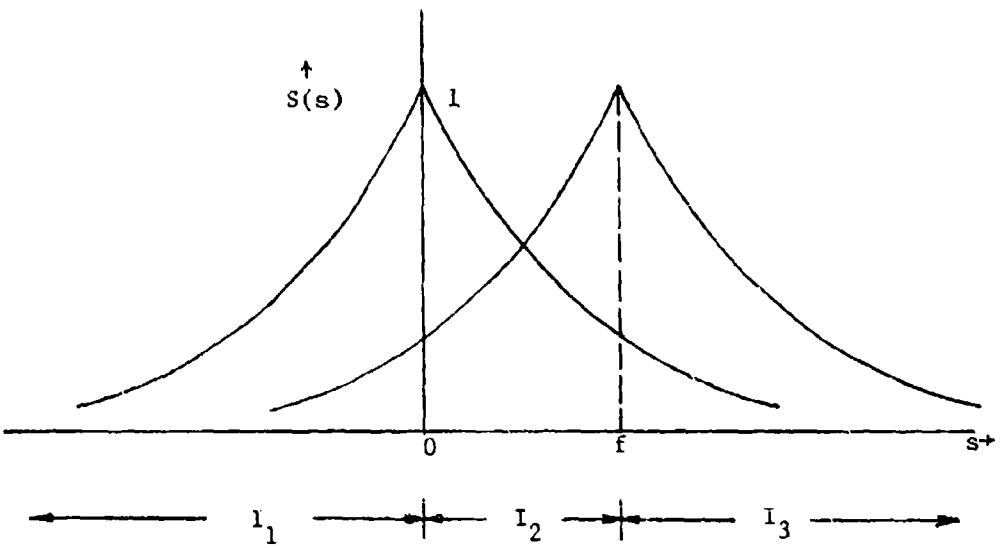

Figure A-1 Integration Regions for Formula A3.

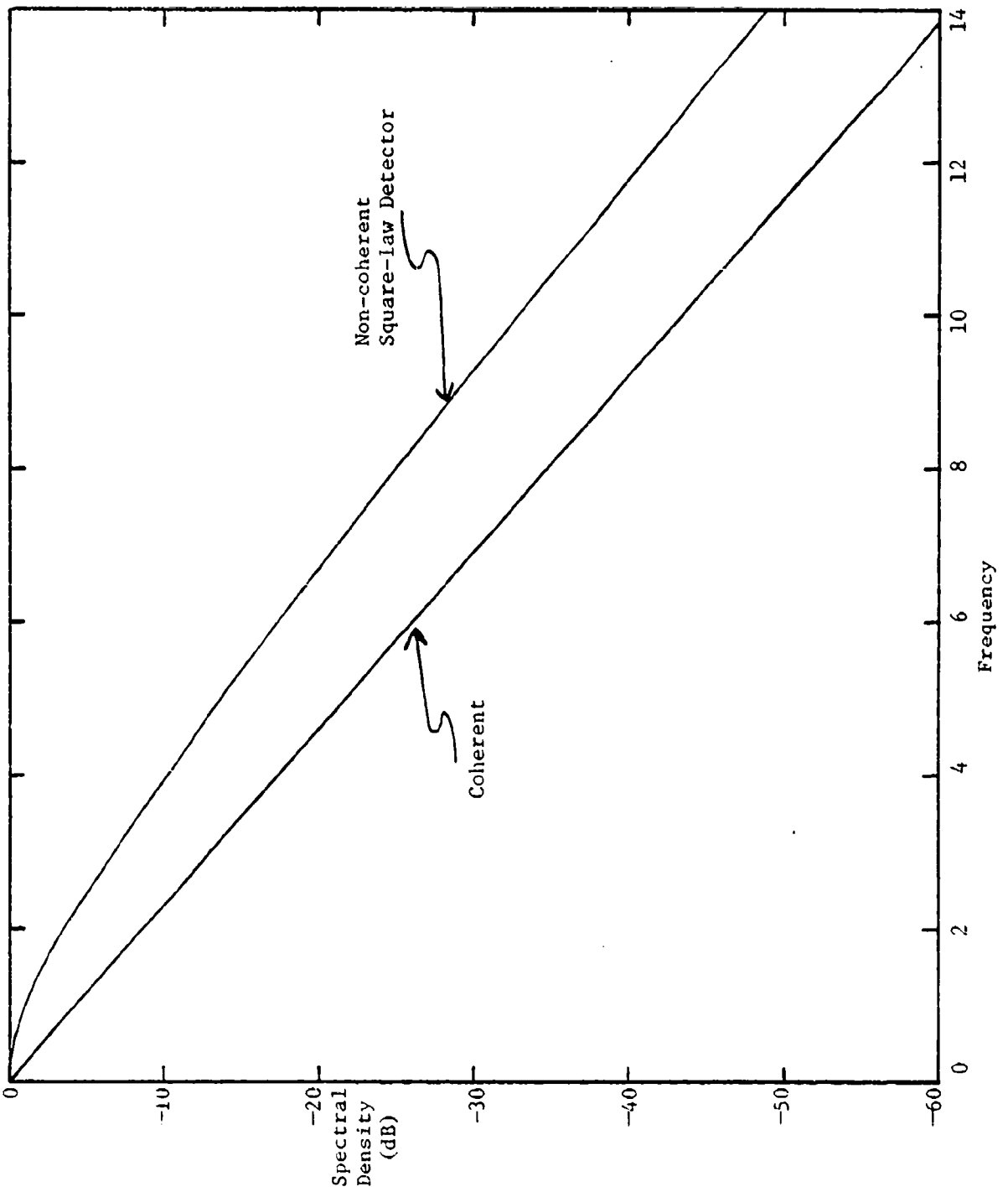

Figure A-2. Noncoherent Spectrum (Square-law detector) of Exponential-Spectrum Clutter.

A.2 LINEAR ENVELOPE DETECTOR

For the linear envelope detector, no formula for the video spectrum exists directly in terms of the coherent spectrum. Rather, the auto correlation functions must be used. Papoulis derives a formula for the autocorrelation of the linear-detected video signal $R_L(\tau)$ in terms of the autocorrelation function of the coherent signal $R_c(\tau)$ when that signal is a Gaussian distributed stationary process [A-1].

$$\sin(\alpha) = R_c(\tau)/R_c(0) \tag{A-5}$$

$$R_L(\tau) = \frac{2}{\pi} R_c(0) \left(\cos(\alpha) + \alpha \sin(\alpha)\right) \tag{A-6}$$

Note that because the coherent signal has zero mean, as τ varies from zero to large values, α varies from $\pi/2$ to approach zero. Thus, one sees that $R_L(\tau)$ contains a dc component such that for large τ, $R_L(\tau)$ approaches $2/\pi$ $R_c(0)$. By subtracting this term from the autocorrelation, the auto covariance of the video spectrum is found.

$$C_L(\tau) = \frac{2}{\pi} R_c(0) \left(\cos(\alpha) + \alpha \sin(\alpha) - 1\right) \tag{A-7}$$

Consider a coherent signal whose spectrum is exponential. Then it has an autocorrelation function of the form:

$$R_{ce}(\tau) = R_{ce}(0) \cdot \frac{1}{1 + \sigma^2\tau^2/2}, \tag{A-8}$$

in which the width constant σ has been so defined by analogy with the classical Gaussian parameter. The Fourier transform of A-8, which represents the coherent spectrum, is [e.g. A-3]

$$S_{ce}(f) = R_{ce}(0) \frac{\pi}{\sqrt{2}\,\sigma} \exp\{2\pi\sqrt{2}\, f/\sigma\}. \tag{A-9}$$

No formula exists for the Fourier transform of Formula A-6 or A-7 under a substituation of Formula A-8 in A-5. Therefore, the spectrum of the non-coherent video signal must be evaluated numerically. This has been done for both the coherent and non-coherent autocovariance functions, and the results are plotted in Figure A-3. A value of $\tau=1$ was used in Formulas A-8, and the frequency scale in Figure A-3 corresponds to this choice.

A-1 The Fourier Integral and Its Applications, A. Papoulis, McGraw-Hill Book Company, Inc., 1962

A-2 Probability, Random Variables, and Stochastic Processes, A. Papoulis, McGraw-Hill Book Company, Inc., 1965

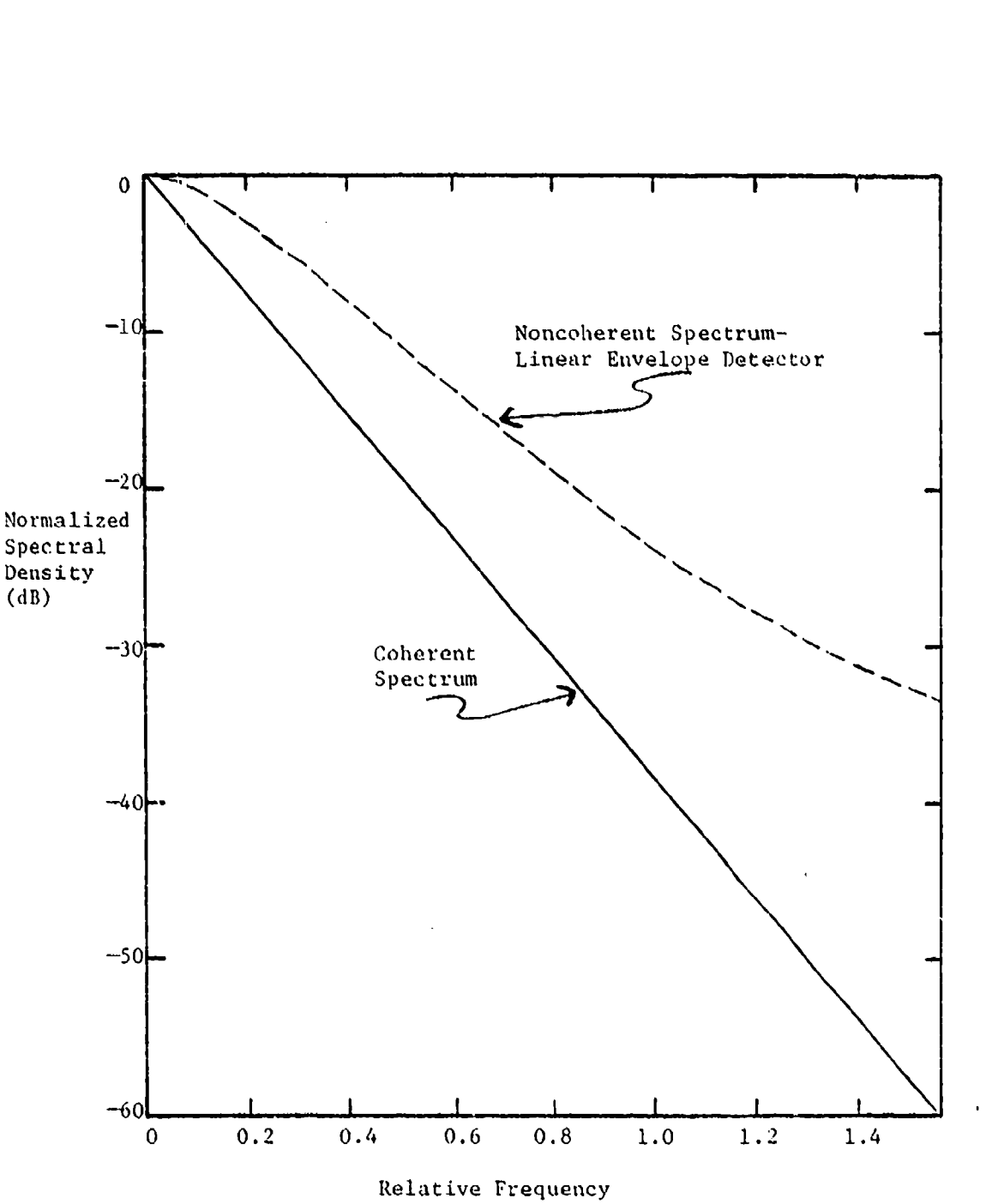

Figure A-3. Noncoherent spectrum for linear envelope detector corresponding to an exponential coherent spectrum.

APPENDIX B

MTI IMPROVEMENT FACTORS

Ward quotes [B-1] the IEEE definition of MTI Improvement Factor (IF): "The signal-to-noise ratio at the output of the system divided by the signal-to-noise ratio at the input of the system averaged uniformly over all target radial velocities of interst." Here binomial-weighted MTI cancellers are assumed to constitute the "system". The IF for cancellers operating on 3 and 4 pulses is given by the following expressions. [B-2]

3-Pulse Canceller:

$$IF = (6 - 8\ \rho(T_r) + 2\ \rho(2T_r))/6 \qquad \text{(B-1)}$$

4-Pulse Canceller:

$$IF = (20 - 30\ \rho(T_r) + 12\ \rho(2T_r) - 2\ \rho(3T_r))/20 \qquad \text{(B-2)}$$

The IF for these two filters will be compared when fed with four different hypothetical clutter spectra. The typifying spectra chosen are listed in Table B-1. They have all been defined to have the same -3 dB point. The shape of the exponential spectrum near zero modulation frequency is typical of empirical spectra. The tails of empirical spectra at higher modulation frequencies lie between the f^{-2} and f^{-4} examples. The Gaussian spectrum is included because of its historical importance.

The results of computing IF using Formulas B-1 and B-2 are shown in Figures B-1 and B-2, respectively. The abscissa variable is the product of interpulse period, T_r, and the parameter ω_3, the -3 dB point of the spectrum. By comparing the corresponding curves for the 3-pulse canceller with those for the 4-pulse case, these features are found. For the Gaussian spectrum, one sees the distinct difference in slope of IF vs $T_r\omega_3$ beginning at about $T_r\omega_3 = 1$. For this spectrum, large difference in IF would be seen from cancellers with 3 and 4 pulses, when $T_r\omega_3$ is small.

For the exponential spectrum, there is also a change in slope, but it begins only below about $T_r\omega_3 = 0.2$. Because of the distinctly different shape of the peaks of the spectral functions, the IF curve for the exponential spectrum is shifted toward lower values of $T_r\omega_3$ by a factor of 2-3.

Both the f^{-2} and f^{-4} curve show no change in slope with increase in number of pulses cancelled. These spectra bound the expected shape of tails of empirical clutter spectra. If the optimistic f^{-4} tail is assumed, a binomial-weighted 4-pulse MTI canceller increases IF by about 3 dB for all $T_r\omega_3$ below about 0.1, compared to a 3-pulse canceller.

Two conclusions appear warranted from this information.

- Misinterpretation of the shape of clutter spectra peaks in the past may have caused both an incorrect estimate of the appropriate spectrum standard deviation constant for use in MTI calculations and an optimistic assessment of MTI IF performance that would be acheived in given clutter conditions.

- Binomial weights for MTI cancellers are a poor choice to deal with spectra having enhanced tails at higher modulation frequencies.

REFERENCES

B-1 "Clutter Filter Performance Measures," H. R. Ward, IEEE International Radar Conference Proceedings, 1980.

B-2 "Gain, Attenuation, and Correlation due to an MTI," R. LaFrance, TSC-W28-2312, 8 November 1978.

TABLE B-1 FOUR EXEMPLARY SPECTRUM FUNCTIONS

Spectrum Type	Spectrum, $S(\omega)$=	Autocorrelation, $\rho(\tau)$-	-3dB Point, $\omega(S=S(0)/2)$=	0.5 Decorrelation, $\tau_{.5}$=
Gaussian	$\frac{2\sqrt{\pi \ln(2)}}{\omega_3} \exp(-\ln(2)(\omega/\omega_3)^2)$	$\exp(-\tau^2\omega_3^2/(4\ln(2)))$	ω_3	$2\ln(2)/\omega_3$
Exponential	$\frac{\pi \ln(2)}{\omega_3} \exp(-\ln(2)\,\omega/\omega_3)$	$1/(1+(\tau\omega_3/\ln(2))^2)$	ω_3	$\ln(2)/\omega_3$
f^{-4}	$2\sqrt{2}/(\omega_3(1+(\omega/\omega_3)^4))$	$\sqrt{2}\exp\left(-\left\lvert\frac{\tau\omega_3}{\sqrt{2}}\right\rvert\right)\sin\left(\pi/4+\frac{\tau\omega_3}{\sqrt{2}}\right)$	ω_3	$1.0135\sqrt{2}/\omega_3$
f^{-2}	$2/(\omega_3(1+(\omega/\omega_3)^2))$	$\exp(-\tau\omega_3)$	ω_3	$\ln(2)/\omega_3$

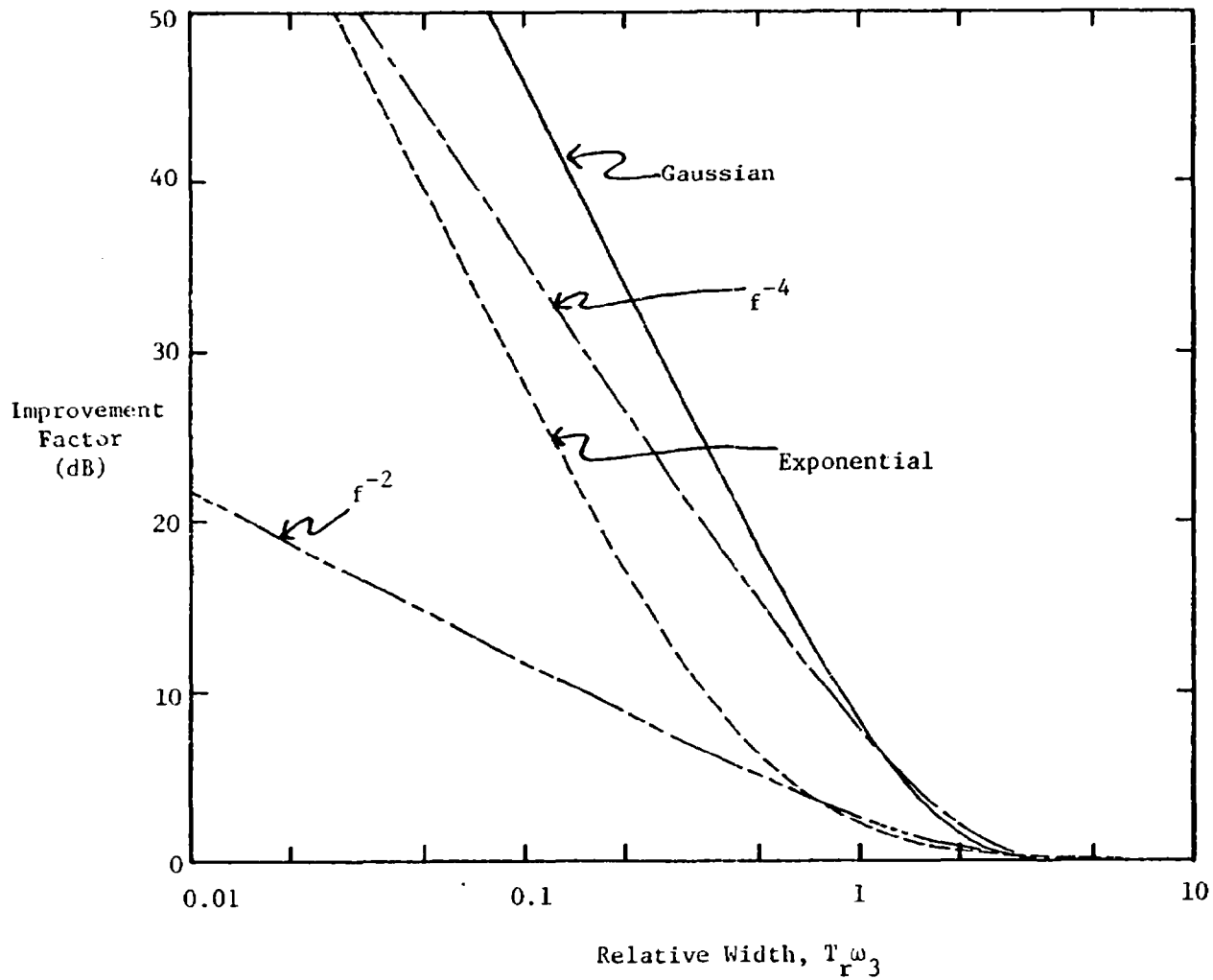

Figure B-1 Improvement Factor for a 3-pulse Binomial-Weight Canceller. Spectrum Types are Defined in Table B-2

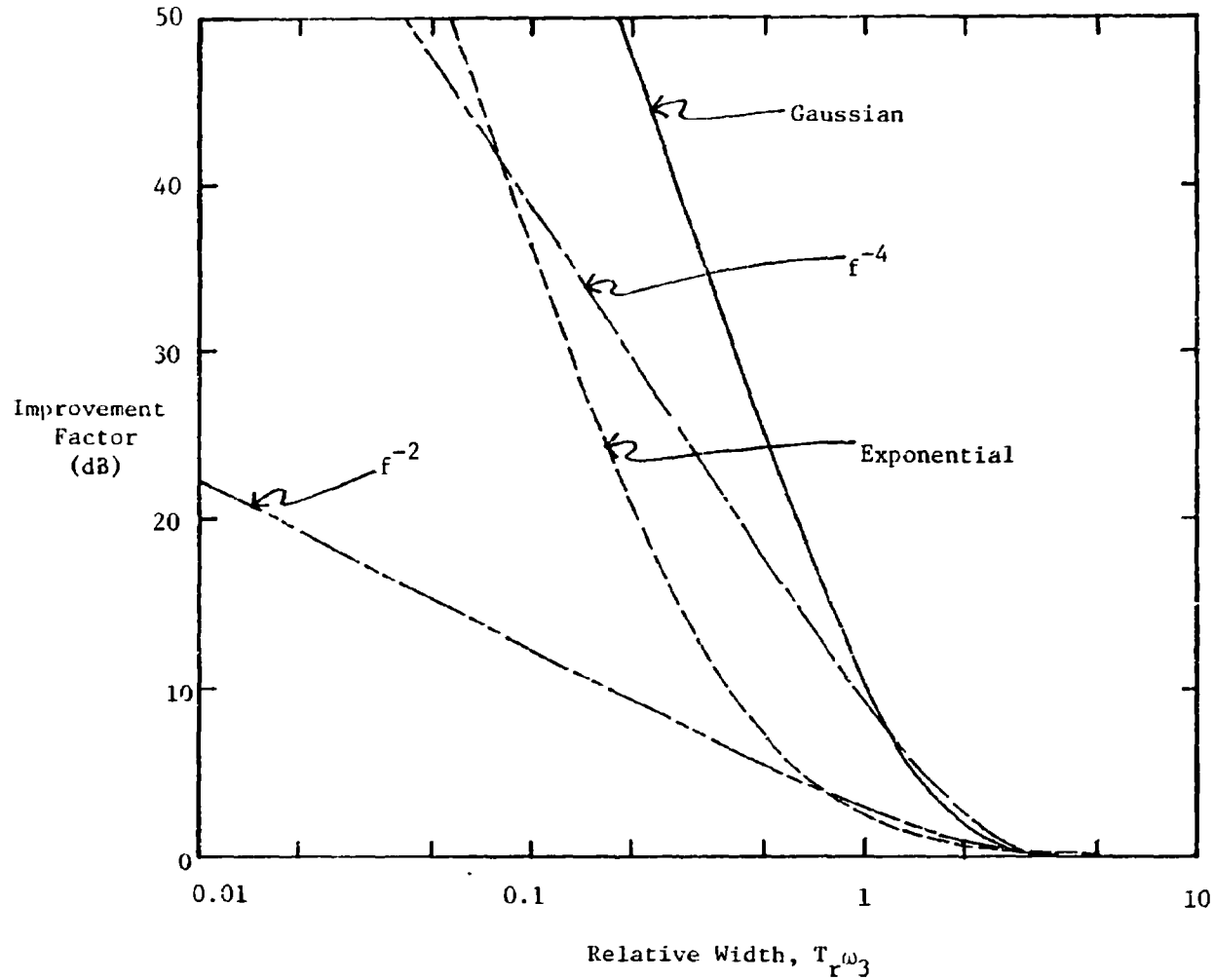

Figure B-2 Improvement Factor for 4-Pulse Binomial-Weight Canceller. Spectrum Types are Defined in Table B-1

APPENDIX C

PHYSICAL ACCEPTABILITY OF HYPOTHETICAL SPECTRUM MODELS

It is convenient to represent empirical spectra in terms of approximating functions that have nice mathematical properties. When talking about random physical processes and representing their fluctuation behavior in terms of these selected analytic spectral functions, one should take care that those functions do not introduce future difficulties, or at least be aware of the difficulties. Examples of difficulties include: infinite power in the process; causal contradiction; and nonexistence of derivatives of the process. Look at each of these in turn.

We want to watch out for implication of infinite power in a process. Empirical spectra of certain noise processes have appeared to have a form

$$S(f) = S_o/|f|. \qquad \text{(C-1)}$$

But, this spectrum has no Fourier transform because of convergence difficulty near the f=0 limit. It is implied that the power from a source with such a spectrum is infinite, or that the spectrum fails to apply at some small value of f. When attempts to find the cutoff frequency appropriate for some processes have been made, experimenters' patience was exhausted before the - cutoff was found. [C-1] Another example of the contradiction about power is the white-noise spectrum, S(f)=constant, $0<f<\infty$. This leads to the classic ultraviolet catastrophe. [C-2] Clearly the solution to both of these dilemmas is to truncate the spectrum.

The notion of causality implies the following. If the input of a linear system has been zero up to some time t, then its output has also been zero for all time up to t. If the power spectrum of the output of the system is S(f) when its input is broadband noise, then a necessary and sufficient condition that the system is causal is

$$\int_{-\infty}^{\infty} \frac{|\ln (S(f))|}{1 + f^2} \, df < \infty \qquad \text{(C-2)}$$

(This is a modification of the Paley-Wiener criterion, applied here to the power spectrum rather than to the amplitude spectrum. [C-3,-4,-5]). There is certainly no argument about the need for causality in clutter signals. At some prior time the radar was not transmitting. (However, the clutter as a mechanical process may have been going for a longer time.) But no argument attempting to extend time works when we recognize that clutter is not stationary, and its statistics behave approximately in a stationary way only over restricted sample intervals. One might well argue about whether an empirical random process such as radar clutter need be representable by broadband noise passed through a linear network. Again here the argument depends on our need for believing in stationary properties. If we insist on using the notion of spectrum to represent an expectation, rather than a deterministic sample of frequency content, then we must accept the consequencies of the condition of wide-sense stationarity. One of these is that a network exists which, when fed with broadband noise, has as its output a proper realization of the process whose spectrum is the one in Question. [C-3]. Thus, the condition in Formula C-2 should apply.

Consider the implication of the nth derivative of a clutter signal being zero. Then all of the n-k derivatives, k=1..n, are deterministic, not random. Therefore, for the clutter signals to be random processes, all of their derivatives must exist. The autocorrelation function of the derivative of a random process X is

$$R_{\dot{x}\dot{x}}(\tau) = \frac{\partial^2 R_{xx}(\tau)}{\partial \tau^2} \qquad \text{(C-3)}$$

and the power of the derivative is $R_{xx}^{\cdot\cdot}(0)$. Therefore, we require that the even-order derivatives of the autocorrelation function at $\tau=0$ all exist. Furthermore, if the derivative is to have finite power,

$$\int_{-\infty}^{\infty} f^{2n} S(f)df < \infty \qquad \text{(C-4)}$$

must apply for all n. [C=3]

Now, consider simple spectral types, including those used in Appendix B as models for MTI calculations, and apply the 3 tests above to them. Table C-1 summarizes the results.

We learn to tolerate the white-noise model because our attention is always centered on the output of some bandlimiting system, and the system itself tells us where and how to truncate, or roll off, the spectrum and thus relieve the contradiction about power. Representation of empirical spectra with a modified white model always includes the fact of a rolloff, if not the correct shape of it. The 1/f spectrum is more difficult to work with for two reasons. The lower limit at which it would be physically reasonable to truncate the spectrum is generally obscure. And, the variance of the process, and hence the power ascribed to it, is proportional to the measurement time. Thus, such processes are not stationary and the notion of spectrum as expectation is hard to live with.

The Gaussian spectrum is far from satisfying the causal test, but the Exponential is close. That is, spectra of the form

$$S(f) = S_o \exp(-f^{\alpha}) \qquad \text{(C-5)}$$

are acceptable so long as $\alpha<1$. Note that when $\alpha<1$, such spectra have high-frequency tails qualitatively in agreement with empirical clutter spectra, in that both deviate from exponential ($\alpha=1$) in the same direction.

TABLE C-1 TEST OF SIMPLE SPECTRUM FUNCTIONS FOR ACCEPTABILITY

FUNCTION	PROCESS POWER	CAUSALITY	PROCESS DERIVATIVES
S(f)=constant, white noise	Infinite, unless truncate at high frequencies	Passes	Infinite, unless spectrum truncated
$1/\|f\|$	Infinite, unless truncated at low frequencies	Fails	Infinite, unless spectrum truncated at high frequencies
Gaussian	Finite	Fails	Finite
Exponential $\exp(-\|f\|)$	Finite	Fails/(barely)	Finite
$1/(1 + f^2)$	Finite	Passes	Infinite, unless spectrum truncated at high frequencies
$1/(1 + f^4)$	Finite	Passes	Infinte for n >1, unless spectrum truncated at high frequencies

The last two spectral types in Table C-1 have difficulty in meeting the derivative test. The derivatives have infinite power above n=1 and 2, respectively.

Thus, only one type of spectrum discussed so far satisfies all three tests, the modified exponential defined in Formula C-5.

REFERENCES

C-1 A. Van Der Ziel, Noise, Prentice-Hall Inc., 1954.

C-2 H. Nyquist, "Thermal Agitation of Electronic Charge in Conductors," Physical Review, Vol. 32, page 110, July 1928.

C-3 See Reference A-1.

C-4 See Reference A-2.

C-5 See Reference 2.

APPENDIX D

SELECTION OF SPECTRUM WIDTH PARAMETER

For the case of precipitation clutter, the vertical shear properties are well documented. But radar designers need clutter spectral properties to guide selection of MTI and waveform designs. The physical model investigated in Section 3.3 provides the means for relating the wind shear to the clutter Doppler spectrum width. But the path needs the clarification that follows.

We accept that for some stated wind conditions, a value (or range of values) for the vertical shear variance can be agreed upon. Then by Formula 7,

$$\sigma_v^2(\delta z) = \sigma^2|\delta z| \qquad \text{(D-1)}$$

is the variance of the velocity difference, v, between scatterers separated by distance δz, in terms of the Wiener parameter, σ. Therefore, it follows that

$$\sigma^2 = \sigma_v^2 (\delta z)/|\delta z| \qquad \text{(D-2)}$$

can be used to estimate appropriate values of the parameter σ. Alternatively, one might want to use a variation based also on Formula 6. The spectrum computation in Section 3.3 which guides the next steps would apply correctly to both cases provided the spectrum slope parameter as defined by Formula 15, is interpreted in light of the variations seen in Figure 12.

Suppose that an exponential-like spectrum, such as the ones plotted in Figures 11 and 12 and which are associated with Wiener-like velocity fields, suit the radar analyst's needs. By Formula 15, the spectrum in the vicinity of $v = 0$ is for $\sigma_B = 1$

$$S^*(v) \cong -\frac{5}{\sigma} v + \text{constant}. \qquad \text{(D-3)}$$

If v has units of meters/sec and σ units of $m^{1/2}$/sec, then the slope constant must have units of dB/($m^{3/2}$/sec) in order that $S^*(v)$ have units of dB/(m/sec). But v requires calibration, because of the restrictive assumption that the beam height parameter σ_B have value 1. Inspection of Formula 14 shows that the proper calibration is made by replacing v by v/σ_B. This may be done for the abscissas of Figures 11 and 12 and for Formulas 15 and D-3 above. Thus,

$$S^*(v) \cong -\frac{5v}{\sigma\sqrt{\sigma_B}} + C(\sigma, \sigma_B) \qquad \text{(D-4)}$$

has the needed scale factor. The "hidden" units now associated with the factor 5 are dB/$m^{1/2}$.

From D-4 it follows that the 3 dB point on the spectrum occurs at

$$v_{3dB} = 0.6 \sigma\sqrt{\sigma_B} \qquad \text{(D-5)}$$

Thus, by Formula D-2 it follows that

$$v_{3dB} = 0.6\sqrt{\sigma_B}\sigma_v(\delta z)/\sqrt{\delta z}\ , \qquad \text{(D-6)}$$

and in Doppler angular frequency space, where

$$\omega = 4\pi v/\lambda\ , \qquad \text{(D-7)}$$

$$\omega_3 = 2.4\pi\sqrt{\sigma_B}\,\sigma_v(\delta z)/(\lambda\sqrt{\delta z}). \qquad \text{(D-8)}$$

Suppose that a radar has a 3 dB elevation beamwidth (for 2-way propagation) of θ_3. Then by Formula 11 (and the comment following it),

$$\sigma_\theta = \theta_3/(2\ln(2)) = \theta_3/2.355 \ . \qquad \text{(D-9)}$$

At a radar range of R, the height of the beam at its ±3 dB (2-way) points is

$$h_3 = R\theta_3 \ , \qquad \text{(D-10)}$$

from which it follows that

$$\sigma_B = \sigma_h = R\sigma_\theta = R\theta_3/2.355 \ . \qquad \text{(D-11)}$$

By combining D-7 and D-10, the formula

$$\omega_3 = \frac{2.4\pi\sqrt{R\theta_3}\ \sigma_v(\delta z)}{\sqrt{2.355}\ \lambda\ \sqrt{\delta z}} \qquad \text{(D-12)}$$

$$\omega_3 \cong \frac{4.9\sqrt{R\theta_3}}{\lambda}\ \frac{\sigma_v(\delta z)}{\sqrt{\delta z}} \qquad \text{(D-13)}$$

Consider the following numerical example. A typical value for atmospheric vertical shear standard deviation is quoted as 5 m/sec/km$^{1/2}$ [D-1]. Thus, $\sigma_v(\delta z)/\sqrt{\delta z} = 5/\sqrt{1000} = 0.158$ m$^{1/2}$/sec. For a 3.2-cm radar having 2-way elevation-plane beamwidth of 2 degrees viewing a target cell at 50 km range, the Doppler bandwidth for widespread precipitation is

$$\omega_3 \cong \frac{4.9\ \sqrt{50{,}000\ \ .0349}\ \ .158}{.032} = 1010 \text{ radians/sec.}$$

Reference

[D-1] S. L. Valley, Handbook of Geophysics and Space Environments, Air Force Cambridge Research Laboratories, 1965.